Hindawi
Mathematical Problems in Engineering
Volume 2022, Article ID 2464560, 13 pages
https://doi.org/10.1155/2022/2464560

Research Article

Negative Effect Compensation of Disturbance for High-Precision Voice Coil Fast Steering Mirror

Li Xiantao,[1] **Botong Li**,[1] **Lu Wang**,[1] **Jinzhao Li**,[1] **Zhanmin Zhou**,[1] **Chong Li**,[2] **and Bao Zhang**[1]

[1]*Changchun Institute of Optics Fine Mechanics and Physics, Chinese Academy of Sciences, Changchun 130033, China*
[2]*Military Representative Office in Changchun of the Air Force Equipment Department, Changchun 130033, China*

Correspondence should be addressed to Li Xiantao; lixiantao_86@126.com

Received 24 April 2022; Revised 17 July 2022; Accepted 28 July 2022; Published 9 September 2022

Academic Editor: Min Ye

In order to further improve the stability of the composite axis aviation photoelectric stabilization platform, a control method of negative effect compensation of disturbance (NECOD) is proposed and applied to the voice-coil fast steering mirror adjusting the optical path of the platform. The experimental results show that the control accuracy and closed-loop bandwidth of the voice-coil fast steering mirror based on NECOD have been greatly improved, while its advantages of large stroke are not possessed by piezoelectric fast mirror. The experimental results of high-frequency turntable and vibration table show that NECOD proposed in this paper has better antidisturbance performance than DOB and ARC, and its parameters are less and easy to adjust. It is proved that the robustness of NECOD is very strong in the presence of 20% parameter perturbation. The final LOS stabilization accuracy experiment shows that the NECOD voice-coil fast steering mirror proposed in this paper fully meets the performance requirements of high-precision aviation photoelectric stabilization platform, and has high practical value for improving the antidisturbance performance of the control system of aviation photoelectric stabilization platform.

1. Introduction

Aviation photoelectric stabilization platform is widely used in optical reconnaissance and tracking systems in aerospace and aviation fields. Its main function is to isolate the motion interference of the carrier to the aiming device, make the LOS of the aiming device focus on the target stably, and quickly improve the imaging quality [1–3].

However, the distance of investigation in modern war is getting farther and farther, so the requirement of LOS stability accuracy is becoming more and more strict. At present, the most advanced aviation photoelectric stabilization platform adopts composite axis structure and advanced control strategy, and its LOS stabilization accuracy has reached 2 μrad (RMS). The so-called composite axis structure is to install a fast steering mirror (FSM) with micromovement in azimuth and pitch in the main optical path on the basis of the traditional large inertia frame, so as to compensate the primarily stable residual of the frame system and achieve higher precision continued LOS stability [4–6]. According to the driving mode, the fast steering mirror structure can be divided into piezoelectric ceramic type and voice-coil motor type [7–9]. Among them, the driving mode based on piezoelectric ceramics has been favored by researchers because of its high bandwidth and large torque [10]. However, with the increasing engineering demand, the disadvantages of piezoelectric ceramics such as small stroke, high power consumption, and complex driving circuit are gradually highlighted. What is more difficult is that piezoelectric ceramics are extremely sensitive to the humidity of the environment [11], which is not conducive to use in complex and changeable environments. In this regard, the fast steering mirror driven by voice-coil motor just effectively overcomes the above shortcomings, especially its stroke can reach 10°~15°, which is unmatched by piezoelectric ceramic driving mode [12]. This also fully meets the engineering requirements (for example, the image motion compensation in the fast swing scanning process of the aviation photoelectric stabilization platform for ultra-long-distance detection, and the piezoelectric ceramic fast

steering mirror cannot meet the requirements due to its small stroke). Comparing the performance indexes of the two, the voice-coil motor driving mode is only poor in antidisturbance performance compared with the piezoelectric ceramic driving mode, while it is better than the piezoelectric ceramic driving in other aspects, which is determined by the inherent characteristics of the two different structures of voice coil and piezoelectric. It can be seen that how to improve the antidisturbance characteristics of voice-coil fast steering mirror system in complex environment and the robustness to model parameters under the condition of existing structure and sensor accuracy is the key to whether voice-coil motor fast steering mirror can replace piezoelectric ceramic fast steering mirror [13, 14].

In the actual working process, the disturbance in the aviation photoelectric stabilization platform mainly comes from three-dimensional linear motion and three-dimensional angular motion [15, 16]. These six dimensions are orthogonal to each other and there is no coupling between them. The linear motion affects the position control accuracy of the system through the mass unbalance moment of the fast steering mirror relative to the rotation center of the flexure hinge. The magnitude of the mass unbalance moment is linearly related to the vibration acceleration and the center of mass offset force arm. The angular motion affects the stability accuracy of the system through the inertial force of the mirror body (the system needs to drive the mirror and the base at the same acceleration at all times to maintain the relative position stability accuracy between the mirror body and the base). The disturbance torque is linearly related to the angular acceleration of the base and the moment of inertia of the mirror body (refer to the national military standard requirements of aviation photoelectric stabilization platform). Therefore, in order to improve the position stability accuracy of the fast mirror, these two torques need to be effectively suppressed.

In the history of the development of disturbance suppression theory, it can be divided into "active disturbance rejection technology" and "passive disturbance rejection technology". The disturbance suppression ability of "passive anti-interference technology" is directly related to the open-loop gain of the system in the disturbance frequency band, so the frequency range of disturbance suppression is limited by the open-loop crossing frequency of the system [17]. The "active disturbance rejection technology" focuses on the active compensation of disturbance, which is more targeted and independent of the performance of the controlled system. Compared with "passive anti-interference technology", its disturbance suppression ability is superior.

The most prominent feature of the disturbance observer is that all the uncertain factors acting on the controlled object are reduced to "total unknown disturbance", which is estimated and compensated by using the input and output information of the system. There is no need to directly measure the external disturbance and predict the action law of the disturbance. In essence, it completely breaks through the limitations of "absolute invariance principle" and "internal model principle". The representative ones are DOB [18–20] and ADRC [21–24]. However, the observation of disturbance by DOB or ADRC is essentially the reverse solution of the disturbance value according to the result information caused by the disturbance. The necessary condition is that the disturbance has affected the system. Moreover, the observation bandwidth of the disturbance observer is more sensitive to the system measurement noise. The higher the bandwidth, the stronger the influence of the noise. Therefore, the ability to suppress high-frequency disturbances is limited in principle. At the same time, the parameter adjustment of ADRC has always been a thorny problem. If the parameters are not optimal, it is difficult to give full play to the maximum potential of the controller. In addition, the larger the order of the controlled system, the slower the observation speed of the disturbance observer, especially for the high-frequency vibration state of three-dimensional linear motion in the system. Most importantly, the disturbance observer needs to get the accurate model of the system, or the disturbance observation accuracy will decrease, which will reduce the anti-interference ability. In order to improve the performance of the disturbance observer, several researches have been done in recent years. To improve the performance of the PMSM current loop in terms of the speed of response, tracking accuracy, and robustness. Deng et al. proposed a hybrid control strategy by combining the adaptive sliding-mode control and sliding-mode disturbance observer [25]. Junbo came up with a method which is to handle power system model uncertainties when implementing dynamic state estimators [26]. Sun et al. made a composite control design for systems with uncertainties and noise using combined extended state observer and Kalman filter [27].

With the development of modern control theory, such as optimal control, robust control, sliding-mode control, and adaptive control can effectively improve the disturbance suppression performance of the system in theory, but the design is difficult, the calculation is complex, the cost of the control system is high, and the suppression ability of high-frequency disturbance is limited, so it is not easy to be popularized and applied in practical engineering.

Image motion compensation technology can significantly improve the imaging clarity of the platform, but this technology requires the fast steering mirror to have a large stroke, which makes the piezoelectric fast steering mirror incompetent. Although the travel of voice-coil motor fast steering mirror meets the requirements, it is vulnerable to various interferences due to its low bandwidth. In the actual aviation environment, aircraft engine vibration, unstable flight shaking, high and low temperatures, and other factors constantly test the anti-interference ability of the fast steering mirror. In this context, NECOD method is proposed in this paper to improve the performance of the system under the existing hardware conditions. NECOD still has strong anti-interference ability and good robustness in complex environments. Moreover, NECOD method does not depend on the fixed system model but only on the control frequency of the servo loop. The higher the control frequency, the stronger the disturbance suppression ability of NECOD [28].

The experimental results show that compared with the representative adaptive robust control (ARC) and disturbance observer (DOB) control strategies, NECOD is more

Figure 1: Voice-coil fast steering mirror and piezoelectric fast mirror used in the experiment.

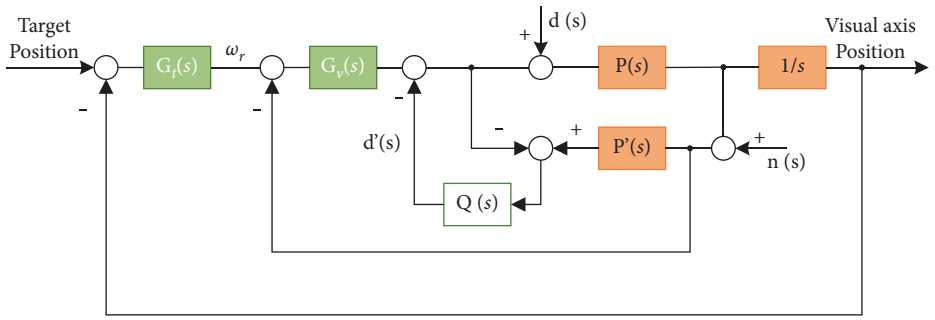

Figure 2: Principle block diagram of DOB.

suitable for the system with both nonlinearity and parameter uncertainty, and the design method is simple and easy to implement, which effectively improves the suppression ability of voice-coil fast mirror to high-frequency disturbances in complex environment and the robustness of parameters. At the same time, through the experimental test of the whole machine, the composite axis aviation photoelectric stabilization platform of voice-coil fast steering mirror based on NECOD control method can improve the stability of the visual axis of the system effectively, which provides an effective support for the comprehensive engineering of voice-coil fast steering mirror.

2. Classical Disturbance Suppression Strategies DOB and ARC

The voice-coil fast steering mirrors used in this experiment are shown in Figure 1. Their stroke is −1.2°~+1.2°. Obviously, this stroke is much larger than the maximum stroke of the piezoelectric fast steering mirror currently used −0.25°~+0.25°.

This system can control three fast steering mirrors at the same time, which is conducive to the subsequent comparison of the three control methods. Each fast steering mirror is a two-axis structure, which is driven by four voice-coil motors at the same time. The position sensor adopts the eddy current sensor.

2.1. Basic Principle of DOB. DOB control method is commonly used in traditional voice-coil fast steering mirror, that is, the disturbance observer is used to observe and compensate the "total disturbance" in the system in real time, so as to suppress the disturbance in the system. Its principle is shown in Figure 2.

Here, $P(s)$ is the actual controlled model of voice-coil fast steering mirror, and $d(s)$ is the voltage equivalent to the "total disturbance" in system. $P'(s)$ is the inverse model of the nominal model of the system, and DOB estimates the "total disturbance" according to the inverse model. The closer its disturbance observation value $d'(s)$ is to the "total disturbance" $d(s)$, the better its disturbance compensation effect is. In the ideal case, the residual disturbance in the system is fully compensated. Then, in the case of ignoring the measurement noise, the above system can be rewritten as

$$\omega(s) = P'(s) \cdot u(s), \tag{1}$$

where $u(s)$ is the control variable obtained by the controller of the fast steering mirror.

However, in practical application, due to the influence of sensor and simulator noise, the disturbance observer can only be compensated through low-pass filter $Q(s)$. In this way, the suppression ability will be strictly limited by $Q(s)$. From Figure 2:

$$\begin{aligned}\omega(s) = {} & \frac{P(s)P'(s)}{P'(s) - (P(s) - P'(s))Q(s)}u(s) \\ & + \frac{P(s)P'(s)(1 - Q(s))}{P\cdot(s) - (P(s) - P\prime(s))Q(s)} \cdot d(s) \\ & + \frac{P(s)Q(s)}{P'(s) - (P(s) - P'(s))Q(s)}n(s).\end{aligned} \tag{2}$$

It can be seen that once the nominal model of the system is determined by the identification method, we can improve the robustness and disturbance suppression ability of the system by designing $Q(s)$.

In order to further analyze the influence of parameter uncertainty on system stability, the modeling error is set as $\widehat{P} = P(s) - P'(s)$, so the closed-loop transfer function is

$$\frac{\omega(s)}{\omega_r(s)} = \frac{G_v(s)P(s)}{\left(1+G_v(s)P'(s)\right)+\left(Q(s)+G_v(s)P'(s)\right)\left(\widehat{P}(s)/P'(s)\right)}. \tag{3}$$

Since the filter $Q(s) \approx 1$ in the frequency domain of the actual operation of the system, in order to realize the robust stability of the system in the whole frequency domain, the model uncertainty must meet:

$$\frac{\widehat{P}(s)}{P'(s)} < \frac{1+G_v(s)P'(s)}{Q(s)+G_v(s)P'(s)} < 1. \tag{4}$$

It can be seen that when DOB disturbance suppression method is adopted, the model uncertainty of the system must not be too large, otherwise it will lead to the instability of the system. However, in the actual working process, the working environment of the aviation photoelectric stabilization platform is very complex and changeable (temperature, electromagnetism, vibration, wind resistance, etc.). Therefore, it is necessary to find a new control method to adapt to the drastic changes of model parameters while ensuring the disturbance suppression ability of the system.

2.2. Adaptive Robust Control. Adaptive robust control combines the dual advantages of adaptive and robust control to meet the application requirements of voice-coil fast steering mirror in complex and changeable application environment [29, 30].

The physical characteristics of voice-coil fast steering mirror can be described as

$$\begin{gathered} \begin{cases} \dot{x}_1 = x_2, \\ J\dot{x}_2 = u(t) + d, \end{cases} \\ J \in [J:\ 0 < J_{\min} < J < J_{\max}], \\ |d| \in D, \end{gathered} \tag{5}$$

where x_1 and x_2 are the position and speed of the mirror relative to the base, J is the moment of inertia of the load, and d is the system disturbance.

The control law is designed based on the sliding mode as

$$u = \widehat{\theta}\dot{q} - k_s s - \eta \cdot \operatorname{sign}(s), \tag{6}$$

where $s = \dot{e} + ce = x_2 - q$, $q = \dot{x}_d - ce$, $e = x_1 - x_d$, $k_s > 0$, $\eta < D$.

Define Lyapunov function as

$$V = \frac{1}{2}Js^2 + \frac{1}{2\gamma}\widetilde{J}^2, \tag{7}$$

where $\widetilde{J} = \widehat{J} - J$, $\gamma > 0$. It is easy to get from equations (10) and (15):

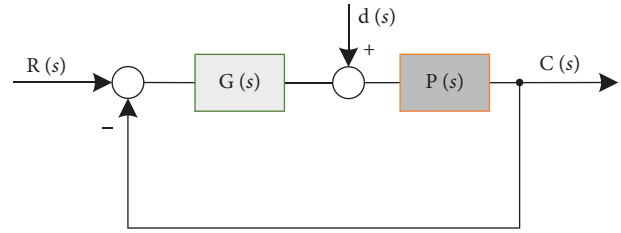

Figure 3: Closed-loop systems with disturbances.

$$\begin{cases} \dot{V} = Js\dot{s} + \dfrac{1}{\gamma}\widetilde{J}\dot{\widetilde{J}} = s\left(J\dot{x}_2 - J\dot{q}\right) + \dfrac{1}{\gamma}\widetilde{J}\dot{\widetilde{J}}, \\ \dot{\widetilde{J}} = -\gamma\dot{q}s. \end{cases} \tag{8}$$

Then,

$$\begin{aligned} \dot{V} &= s(u + d - J\dot{q}) + \frac{1}{\gamma}\widetilde{J}\dot{\widetilde{J}} \\ &= s\left(\widehat{J}\dot{q} - k_s s - \eta \cdot \operatorname{sign}(s)d - J\dot{q}\right) + \frac{1}{\gamma}\widetilde{J}\dot{\widetilde{J}} \\ &= s\left(\widehat{J}\dot{q} - k_s s - \eta \cdot \operatorname{sign}(s)d\right) + \widetilde{J}(\dot{q}s) \\ &= -k_s s^2 - \eta|s| + d \cdot s < -k_s s^2 \le 0. \end{aligned} \tag{9}$$

In order to prevent the signal $u(t)$ from being too large due to too large $\widehat{J}$, the adaptive law is modified as follows:

$$\dot{\widehat{J}} = \operatorname{Proj}_{\widehat{J}}(\gamma\dot{q}s) = \begin{cases} 0, & \text{if} \widehat{J} = J_{\max} \text{ and } > 0, \\ 0, & \text{if} \widehat{J} = J_{\min} \text{ and } < 0, \\ & \text{otherwise} \end{cases} \tag{10}$$

It can be seen that adaptive robust control can significantly suppress the disturbance and model perturbation to ensure the control accuracy of the system. However, from the above controller design process, it is obvious that the controller configuration process is complex, there are many adjustment and setting parameters, and the parameters affect and couple each other, and so it is difficult to achieve optimization in engineering practice.

3. Negative Effect Compensation of Disturbance

In order to improve the disturbance suppression ability of voice-coil fast steering mirror, a control method of disturbance negative effect compensation is proposed in this paper. This method does not depend on any information of the system model, so it is not sensitive to the parameter perturbation of the model. At the same time, because it does not include differential link, it is little affected by the measurement noise of the sensor. In addition, the parameter adjustment of this control method is simple and easy to be realized in practical engineering.

3.1. Analysis of Disturbance Suppression Ability. When there is external disturbance $d(s)$ in the system, the closed-loop system with unit feedback can be expressed as Figure 3.

The transfer function of the system is

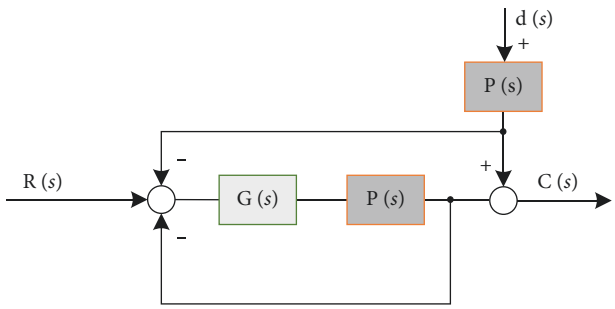

Figure 4: The equivalent block diagram of Figure 4.

$$C(s) = \frac{G(s)P(s)}{1 + G(s)P(s)} R(s) + \frac{1}{1 + G(s)P(s)} d(s)P(s). \quad (11)$$

The error transfer function of the system is

$$E(s) = \frac{1}{1 + G(s)P(s)} R(s) + \frac{1}{1 + G(s)P(s)} d(s)P(s). \quad (12)$$

The first term of $E(s)$ expression is the steady-state error of the system, and the second term is the error caused by torque interference. Suppressing disturbance is to reduce the response of the second term.

The equivalent block diagram of Figure 4 can be represented as follows.

In order to eliminate the influence of disturbance on the system without changing the system gain, two feedback links are introduced in Figure 5.

Here, $1/z$ is the unit delay. If the delay time is τ, the transfer function of the delay link is

$$G_1(s) = \frac{1}{1 - e^{-\tau s}}. \quad (13)$$

If the delay time τ is small, the transfer function of the delay term is expanded by Taylor expansion and the higher order term is ignored:

$$e^{-\tau s} = 1 - \tau s. \quad (14)$$

The transfer function of the system at this time is obtained:

$$C(s) = \frac{G(s)P(s)}{\tau s + (1 + \tau s)G(s)P(s)} R(s) + \frac{\tau s}{\tau s + (1 + \tau s)G(s)P(s)} d(s)P(s). \quad (15)$$

The response of the system to external disturbance $d(s)$ is

$$E(s) = \frac{-\tau s(G(s)P(s) + 1)}{\tau s + (1 + \tau s)G(s)P(s)} R(s) + \frac{\tau s}{\tau s + (1 + \tau s)G(s)P(s)} d(s)P(s). \quad (16)$$

It can be seen from the above formula that the smaller the τ, the smaller the response of the system to the disturbance, that is, the stronger the anti-interference ability of the system. If $\tau \longrightarrow 0$, then:

$$C(s) = R(s), \quad E(s) = 0. \quad (17)$$

At this time, the system principle block diagram can be simplified as Figure 6.

3.2. Measurement Error Analysis. Considering the measurement error $n(s)$ of the sensor, such as the measurement noise in Figure 7.

When $\tau \longrightarrow 0$, the response of the system to $C(s)$ is

$$C(s) = (e^{-\tau s} - 2)\frac{G(s)P(s)}{(1 - e^{-\tau s}) + (2 - e^{-\tau s})G(s)P(s)} n(s) \longrightarrow -n(s). \quad (18)$$

It can be seen that there is no differential term in this control scheme, and the influence of measurement deviation and high-frequency noise on the system output will not be amplified.

3.3. Analysis on the Influence of Controlled Object Change on System Performance. When there is additive uncertainty δ in the controlled system $P(s)$ as Figure 8:

At this time, the transfer function of the system is

$$C(s) = \frac{(1 + \delta)G(s)P(s)}{(1 - e^{-\tau s}) + (2 - e^{-\tau s})(1 + \delta)G(s)P(s)} R(s) + \left((e^{-\tau s} - 2)\frac{(1 + \delta)^2 G(s)P(s)}{(1 - e^{-\tau s}) + (2 - e^{-\tau s})(1 + \delta)G(s)P(s)} + (1 + \delta) \right) D(s)P(s). \quad (19)$$

The error transfer function of the system is

$$E(s) = \frac{(1 - e^{-\tau s})(1 + \delta)G(s)P(s) + (1 - e^{-\tau s})}{(1 - e^{-\tau s}) + (2 - e^{-\tau s})(1 + \delta)G(s)P(s)} R(s) + \left((e^{-\tau s} - 2)\frac{(1 + \delta)^2 G(s)P(s)}{(1 - e^{-\tau s}) + (2 - e^{-\tau s})(1 + \delta)G(s)P(s)} + (1 + \delta) \right) D(s)P(s). \quad (20)$$

It can be seen from the above formula that when the control period τ is small enough, the parameter perturbation of the controlled system has little impact on the performance of the control system.

The parameter b is introduced into the feedback loop in Figure 9, so that the control scheme can be further optimized and adjusted in combination with the controlled system $P(s)$.

Then,

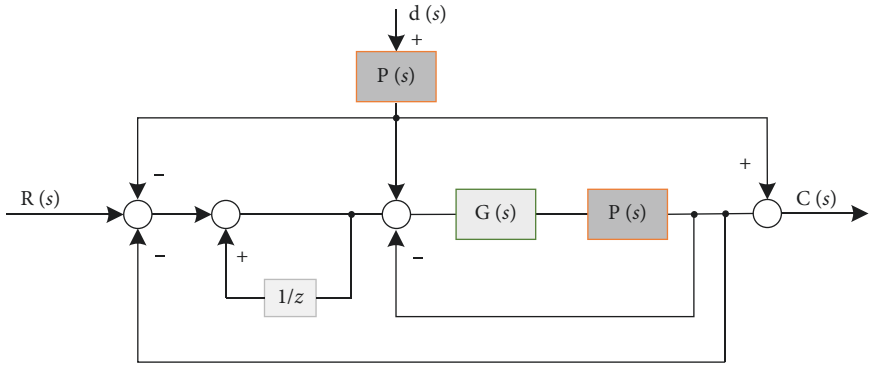

Figure 5: After introducing two feedback links.

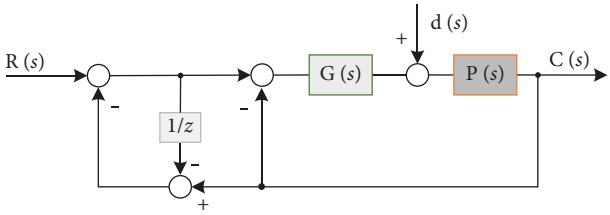

Figure 6: Equivalent block diagram of the system when $\tau \longrightarrow 0$.

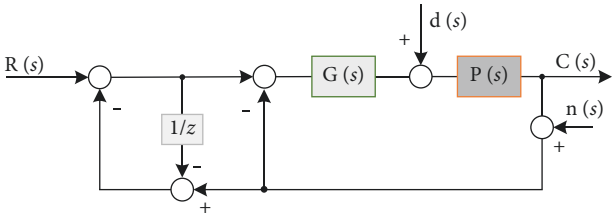

Figure 7: When there is measurement error.

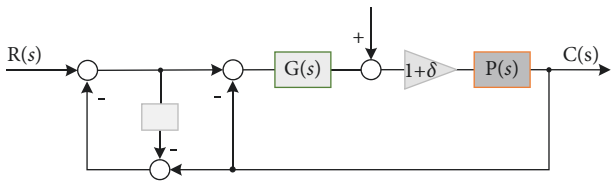

Figure 8: When there is additive uncertainty δ.

$$C(s)=\frac{G(s)P(s)}{(1-b+b\tau s))+(1+b\tau s)G(s)P(s)}R(s)$$
$$+\left((b-b\tau s-2)\frac{G(s)P(s)}{(1-b+b\tau s)+(1+b\tau s)G(s)P(s)}+1\right)d(s)P(s). \tag{21}$$

When $\tau \longrightarrow 0$,

$$C(s)=\frac{G(s)P(s)}{(1-b+b\tau s))+(1+b\tau s)G(s)P(s)}R(s+)$$
$$\frac{(1-b+b\tau s)+(b-1)G(s)P(s)}{((1-b+b\tau s))+(1+b\tau s)G(s)P(s)}d(s)P(s). \tag{22}$$

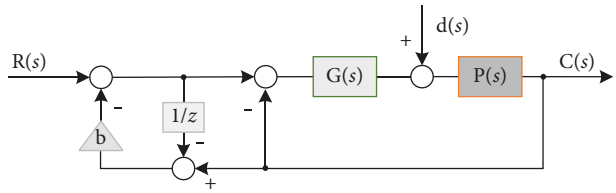

Figure 9: After introducing parameter b.

It can be seen from the above formula that when $b \longrightarrow 1$, the anti-interference ability of the system is stronger, but the value of b is affected by the stability of the system.

Compared with the classical ADRC, the NECOD method has the following advantages.

(1) It is completely independent of the system model and can be designed independently.

(2) No differential link, strong noise adaptability.

(3) Few parameters, simple adjustment, and easy engineering practice.

4. Experimental Result

In order to comprehensively test the performance of NECOD voice-coil fast steering mirror, this paper carries out bandwidth test experiment, disturbance suppression ability experiment, and parameter perturbation adaptability experiment. As a comparison, DOB-type voice-coil fast steering mirror, ARC-type voice-coil fast steering mirror, and piezoelectric fast steering mirror have also carried out the above test experiments.

In the experiment, the parameters of the PI controller are set as $405s + 603/s$. And we obtain the controlled model approximately as $1.85 \times 10^5/s^2 + 10^4 s + 4.2 \times 10^4$ by the way of frequency sweeping identification on the voice-coil fast steering mirror, then we design the $P'(s)$ according to the controlled model. As for the ARC method, we set the parameters as 0.1 and 0.04.

4.1. Bandwidth Test Experiment. In order to test the closed-loop bandwidth performance of NECOD voice-coil fast steering mirror, ARC voice-coil fast steering mirror, and DOB voice-coil fast steering mirror, frequency sweeping

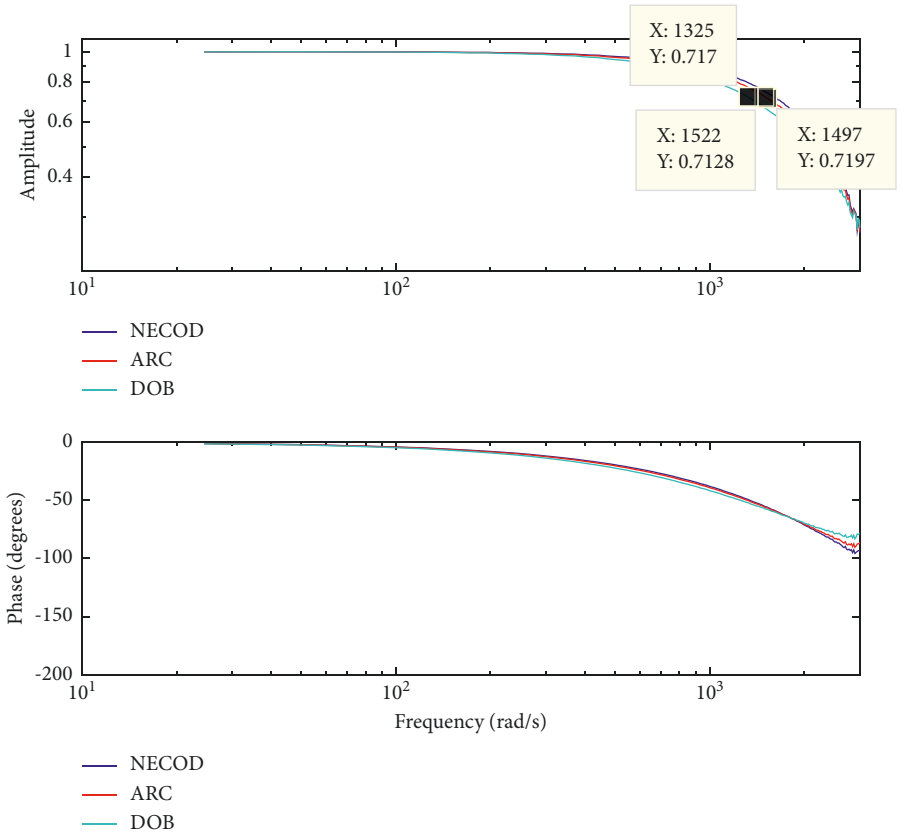

Figure 10: The bandwidth testing of FSM.

experiments have been done to the three kinds of fast steering mirrors. And the results are shown in Figure 10:

In order to test the closed-loop bandwidth performance of NECOD voice-coil fast steering mirror, ARC voice-coil fast steering mirror, and DOB voice-coil fast steering mirror, the piezoelectric fast steering mirror that has been produced by PI company is used as the benchmark, and the three are installed in the optical path at the same time. The specific installation results are shown in Figure 10.

In this experiment, the input signal with a frequency of 1–500 Hz was inputted into the fast steering mirror closed-loop control system, and the system bandwidth can be obtained by drawing the closed-loop Bode diagram curve shown in Figure 11.

After testing, the closed-loop bandwidth achieved by the three control strategies can reach more than 200 Hz, which is basically equivalent to the bandwidth performance of the formed product piezoelectric fast mirror, and fully meets the needs of the aviation photoelectric stabilization platform in practical work.

4.2. Test on Disturbance Suppression Ability of Angular Motion. In order to compare and test the disturbance isolation ability of the three control methods for angular motion, NECOD voice-coil fast steering mirror, ARC voice-coil fast steering mirror, DOB voice-coil fast steering mirror, and piezoelectric fast steering mirror are installed in the high-frequency turntable. In the following figure, 1, 2, 3, and 4 represent the above four kinds of fast steering mirrors, respectively. In the experiment, make the four steering mirrors in the zero locking state, and then make the high-frequency turntable rotate within the frequency of 50 Hz and conduct a rotation comparison experiment every 2 Hz. During the continuous rotation of the turntable, the maximum position fluctuation data of four fast steering mirrors relative to the zero point are collected at the same time. Figure 11 shows the angle fluctuation of four fast mirrors

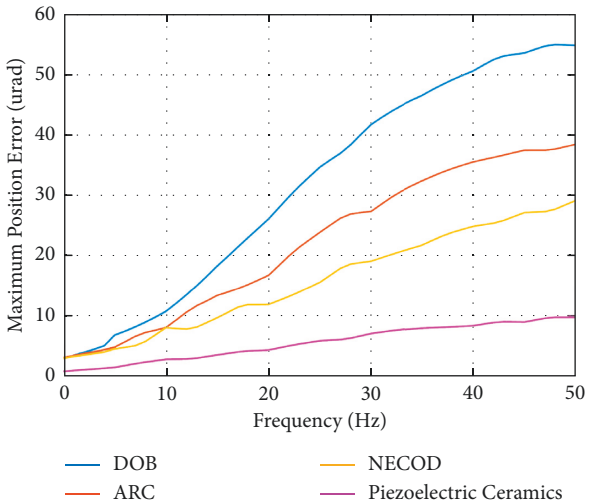

Figure 11: Experimental results of angular motion.

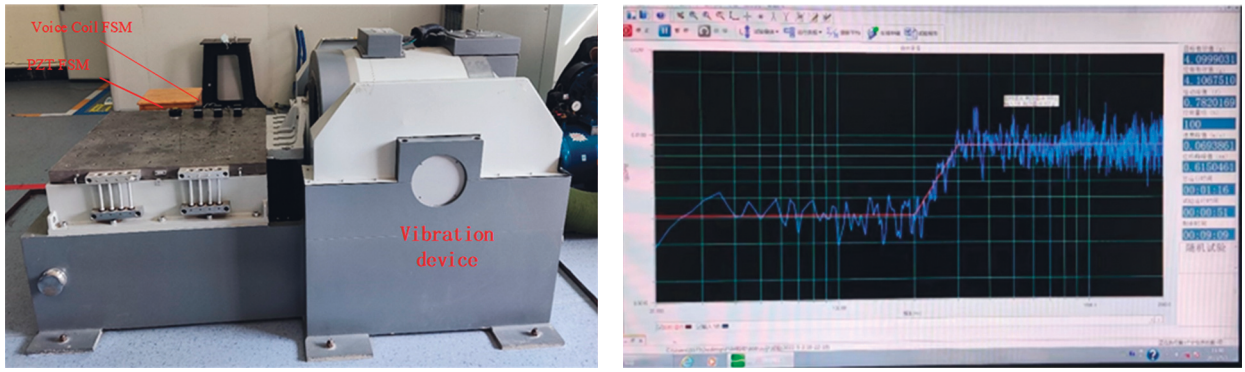

(a) (b)

Figure 12: The disturbance suppression capability test under vibration conditions.

under the influence of arbitrary frequency disturbance within 50 Hz.

It can be clearly seen that under the influence of disturbance within 50 Hz, the disturbance suppression ability decreases gradually with the increase of disturbance frequency. From the results of performance comparison, the piezoelectric fast steering mirror has the strongest disturbance suppression ability and the voice-coil fast steering mirror has weak disturbance suppression ability. The disturbance suppression ability of NECOD voice-coil fast steering mirror and ARC voice-coil fast steering mirror is slightly higher, which are generally equal, that is, the disturbance suppression ability of NECOD and ARC needle within 50 Hz is roughly the same.

4.3. Test of Disturbance Suppression Ability Caused by Linear Motion. In order to compare and test the disturbance suppression ability of four kinds of fast steering mirrors to linear motion, they are installed in the shaking table at the same time. The specific installation results are shown in Figure 12.

In the experiment, make the four steering mirrors still in the zero locking state, and then make the vibration table vibrate randomly with the vibration order of 4.2 g within the frequency of 15–2000 Hz. The vibration power spectrum of the shaking table is shown in the above figure *b*.

In the process of random vibration, the position fluctuation data of four kinds of fast steering mirrors relative to the zero point are collected at the same time, as shown in Figure 13.

It can be clearly seen that under the influence of random vibration within 2000 Hz, the disturbance suppression ability of piezoelectric fast steering mirror is the strongest and the range of position fluctuation is the smallest, which is closely related to the structural properties of piezoelectric driving mode. Among the three kinds of voice-coil fast steering mirrors, the position fluctuation of NECOD fast steering mirror is the smallest, ARC fast steering mirror is the second and DOB fast steering mirror is the largest. It can be seen that the NECOD control method has a stronger ability to suppress high-frequency disturbances. The reason is that there are few intermediate links in the NECOD control method, which is directly related to the control cycle. Therefore, the lag of the disturbance reverse suppression component in the control quantity is small, the real-time performance is higher, and the disturbance suppression ability is stronger. The ARC control method has many intermediate links, and the phase delay of the disturbance reverse suppression component in the control quantity is large, which affects the disturbance suppression effect. In the DOB control method, due to the inevitable differential link in the inverse model, especially the fast steering mirror is a second-order controlled model, the second-order differential will greatly amplify the measurement noise, limit the fitting bandwidth of the disturbance observer, and then limit the ability to suppress high-frequency disturbances.

4.4. Parameter Robustness Experiments. To verify the effect of parameter perturbation on controller performance, change the motor drive factor $\Delta = \pm 20\%$ while keeping the three voice-coil fast steering mirror designed controllers unchanged (that is, to change the model parameters of the controlled object). Then, bandwidth, three-dimensional angular motion, and three-dimensional linear motion experiments are reconducted, and the control performance of NEODC, ARC and DOB voice-coil fast steering mirror is compared before and after adjusting parameters. The experimental results are shown in Tables 1–3.

It can be seen from the above experiments that the performance of DOB voice-coil fast steering mirror changes greatly, while ARC voice-coil fast steering mirror and NEODC voice-coil fast steering mirror have strong robustness against model parameter perturbation of the system model and meet the performance requirements in practical projects.

4.5. Line-of-Sight Pointing Accuracy Test. In order to test the actual application effect of NEODC voice-coil fast steering mirror, ARC voice-coil fast steering mirror, DOB voice-coil fast steering mirror, and piezoelectric-fast steering mirror in the actual composite axis aviation photoelectric stabilization platform, the four are installed in the designed optical system and the whole machine line-of-sight pointing experiments are carried out. The experimental principle is as Figure 14:

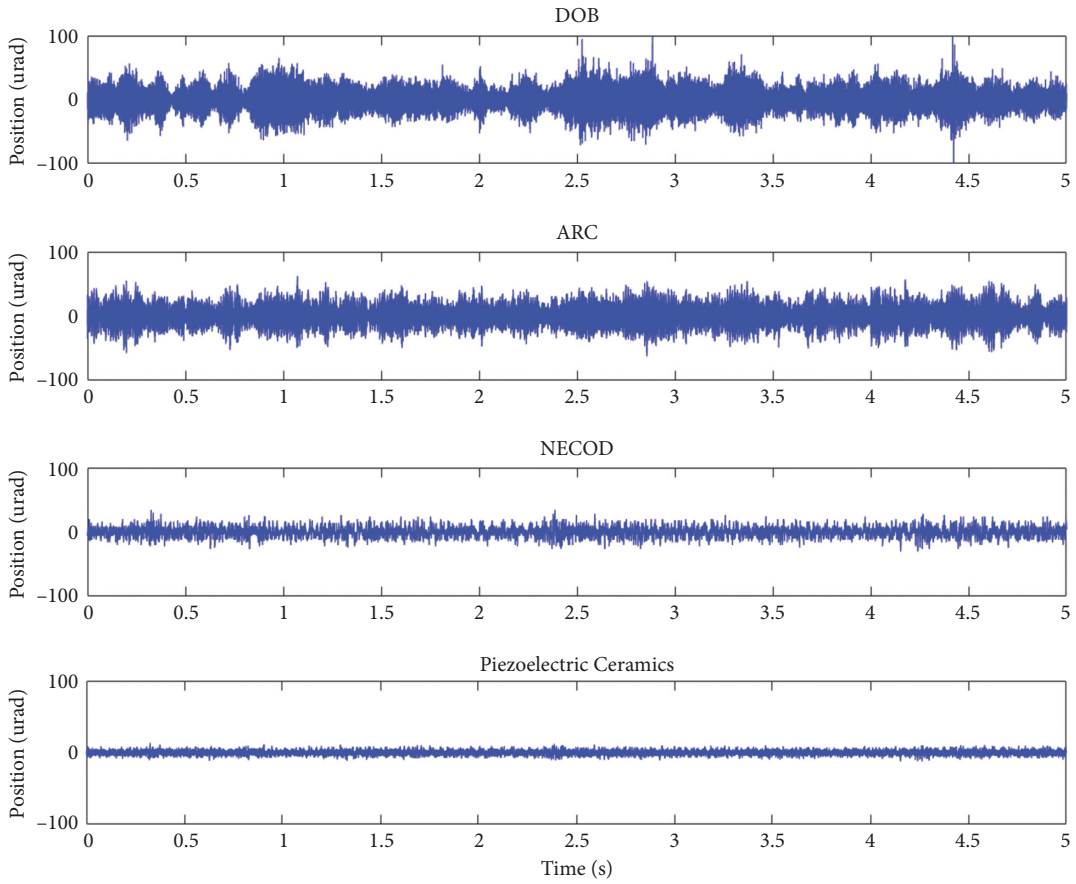

Figure 13: Experimental results of linear motion.

Table 1: Effect of model parameter changes on system bandwidth.

	Original bandwidth (Hz)	Bandwidth when $\Delta = 20\%$ (Hz)	Bandwidth when $\Delta = -20\%$ (Hz)
DOB	230	209	206
ARC	250	234	232
NECOD	265	256	253

Table 2: Maximum position fluctuation under 50 Hz random rotation.

	Original maximum position fluctuation (μrad)	Maximum position fluctuation when $\Delta = 20\%$ (μrad)	Maximum position fluctuation when $\Delta = -20\%$ (μrad)
DOB	55	63	61
ARC	38	41	42
NECOD	29	33	30

Table 3: Maximum position fluctuation under random vibration.

	Original maximum position fluctuation (μrad)	Maximum position fluctuation when $\Delta = 20\%$ (μrad)	Maximum position fluctuation when $\Delta = -20\%$ (μrad)
DOB	101	117	115
ARC	62	66	65
NECOD	31	35	32

4.5.1. Line-of-Sight Pointing Accuracy Test under Angular Disturbance. To test the effect of three-dimensional angular motion on the line-of-sight pointing accuracy of the aeronautical photoelectric stabilization platform, the framework of the aviation photoelectric stabilization platform is installed in the flight simulation turntable to track the target stably. The experimental device is shown in Figure 15.

During the experiment, the flight simulator performs an airplane simulation flight test every 1 Hz within 15 Hz. With the same primary stability accuracy of the frame, four kinds

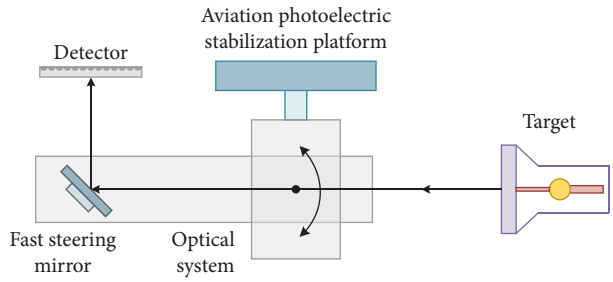

Figure 14: Line-of-sight pointing accuracy test.

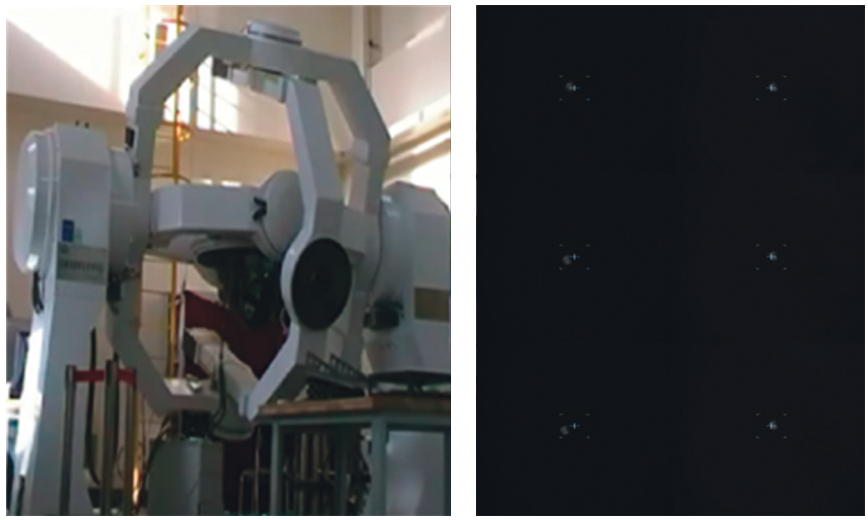

(a) (b)

Figure 15: Angular perturbation experiment.

of fast steering mirrors are used to compensate the continued stability residuals of the frame in the optical system. Under the condition of disturbance, we continuously collected the motion video of the visual axis of the optical system relative to the target for 15 minutes, and then calculated the variance of the target shaking relative to the center of the field of view by image analysis.

The above picture *b* is taken from the video. The left side is the one with poor stability and accuracy of the boresight. It has a large amount of shaking relative to the center of the reticle, while the right side has a small amount of shaking relative to the center of the reticle. At each disturbance frequency, the stability accuracy of the platform's line-of-sight is shown in Figure 16.

As can be seen from the above figure, due to the existence of stable first-order frame, the line-of-sight accuracy of piezoelectric-fast steering mirror is the highest within the frequency range of 15 Hz, followed by NEODC-voice-coil-fast reflector, ARC-voice-coil-fast reflector, and DOB-voice-coil-fast reflector, but they are not different from each other much, which are far less than 5 μrad (RMS), and completely meet the needs of actual projects.

4.5.2. Line-of-Sight Pointing Accuracy Test under Linear Disturbance. In order to test the effect of linear motion on the

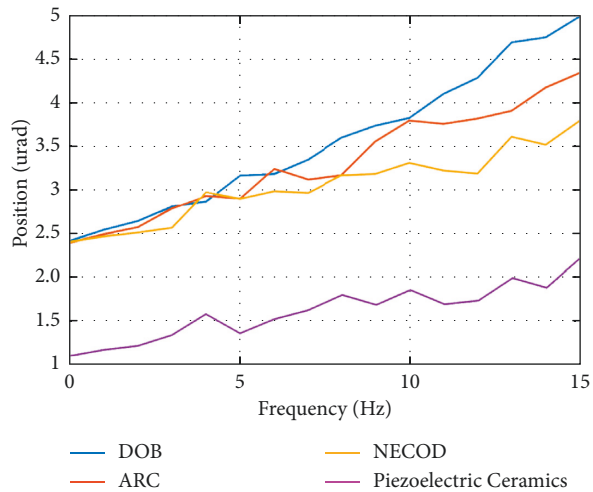

Figure 16: Experimental results of angular motion.

line-of-sight pointing accuracy of the aviation photoelectric stabilization platform, the aviation photoelectric stabilization platform is installed in a vibration table and the target is tracked. The experimental environment is shown in Figure 17.

During the experiment, the vibration table also vibrates with the power spectrum shown in Figure 12. Four kinds of fast steering mirrors are used to compensate the primary

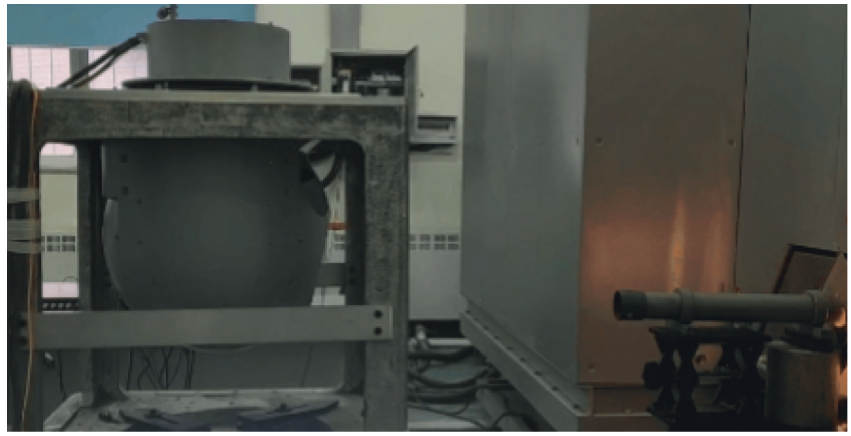

Figure 17: Linear perturbation experiment.

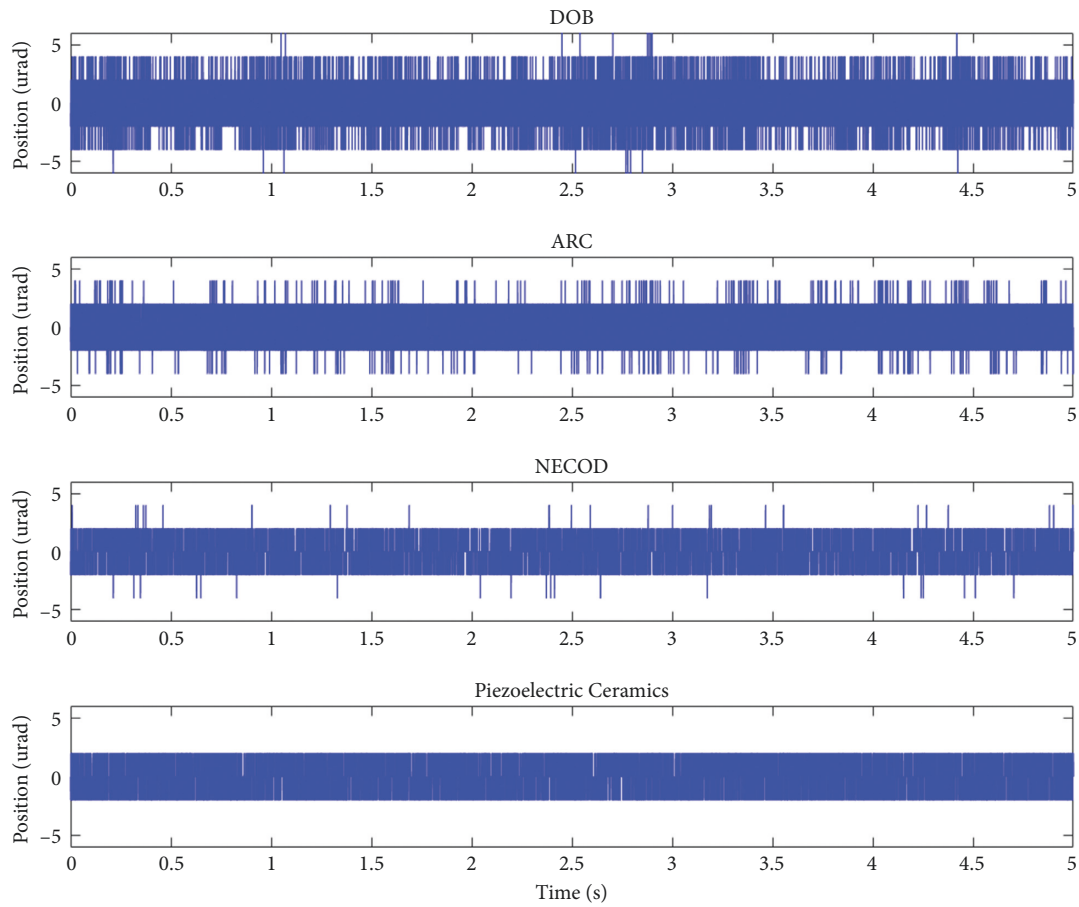

Figure 18: Vibration experiment results.

stability residuals of the frame in the optical system with the same primary stability accuracy in order to achieve the continued Los stability of the aviation photoelectric stabilization platform.

By collecting the deviation of the target relative to the central point of the visual axis, the shaking of the visual axis relative to the inertial space under the condition of vibration is tested, so as to compare and test the visual axis stability accuracy of the composite axis aviation photoelectric stabilization platform.

Figure 18 shows the real-time stable tracking of the target by the aviation photoelectric stabilization platform under the condition of vibration. Due to the comprehensive application of shock absorber, beam reduction ratio of lens group in optical system, and control algorithm, the influence of vibration on the LOS stability accuracy of the system is

reduced. It is obvious from the data in the figure that the piezoelectric fast steering mirror has the best visual axis stability effect, followed by NECOD, followed by ARC voice-coil fast steering mirror, and DOB voice-coil fast steering mirror, but all are far less than 5 μrad (RMS).

5. Conclusion

In order to further improve the performance of the composite axis aviation photoelectric stabilization platform, a NECOD voice-coil fast steering mirror system is proposed. Compared with ARC voice-coil fast steering mirror system and DOB voice-coil fast steering mirror system, it has stronger suppression ability for high-frequency disturbance, strong robustness, few control parameters, easy adjustment, and optimization, and is suitable for engineering implementation. Compared with the piezoelectric fast steering mirror system, it not only has almost the same level of disturbance suppression ability and bandwidth as the piezoelectric fast steering mirror but also has larger stroke, simpler driving circuit, and lower power consumption.

In this way, it overcomes the shortcomings of weak high-frequency disturbance suppression ability and poor parameter robustness of the traditional voice-coil fast steering mirror. While ensuring the line-of-sight pointing accuracy of the composite axis aviation photoelectric stabilization platform, it effectively improves the maximum stroke of the system, simplifies the driving circuit and reduces the power consumption.

In the experiment of the composite axis aviation photoelectric stabilization platform based on NECOD voice-coil fast steering mirror, its parameters meet the requirements of practical application, its line-of-sight pointing accuracy can achieve 5 μrad (RMS), and the maximum travel can reach -1.2°~1.2°. NECOD voice-coil fast steering mirror has strong parameter robustness, few parameters, and easy engineering implementation. It provides a strong support for its engineering application in the composite axis aviation photoelectric stabilization platform and has high reference value and application value.

Data Availability

The datasets used and analyzed during the current study are available from the corresponding author upon reasonable request.

Conflicts of Interest

The authors declare that they have no conflicts of interest.

Acknowledgments

This work was funded by general program of National Natural Science Foundation of China (no. 61675202).

References

[1] J. C. Fang, Q. I. Zi-Hui, and M. Y. Zhong, "Feedforward compensation method for three axes inertially stabilized platform imbalance torque," *Journal of Chinese Inertial Technology*, vol. 18, 2010.

[2] Y. Zhang, T. Yang, C. Li et al., "Fuzzy-PID control for the position loop of aerial inertially stabilized platform," *Aerospace Science and Technology*, vol. 36, pp. 21–26, 2014.

[3] J. M. Hilkert, "Inertially stabilized platform technology Concepts and principles," *IEEE Control Systems*, vol. 28, no. 1, pp. 26–46, 2008.

[4] D. J. Kluk, *An Advanced Fast Steering Mirror for Optical communication*, Massachusetts Institute of Technology, Cambridge, Massachusetts, USA, 2007.

[5] L. R. Hedding, "Fast Steering Mirror Design and Performance for Stabilization and Single axis scanning," *Acquisition, Tracking, and Pointing IV*, vol. 1304, 1990.

[6] M. R. Suite, H. R. Burris, and C. I. Moore, "Fast Steering Mirror Implementation for Reduction of Focal-Spot Wander in a Long-Distance Free-Space Optical Communication link," *International Society for Optics and Photonics*, vol. 5160, pp. 439–446, 2004.

[7] L. Ning, D. Chen, and C. Guan, "Two-dimension piezoelectrical fast steering mirror," *Opto-Electronic Engineering*, vol. 22, no. 01, pp. 51–60, 1995.

[8] J. Zhou, H. Yin, Y. Wang, and G. Jin, "Research on Shaftless Fast-Steering Mirror Used in a Precision Tracking-Aiming system," *Proceedings of SPIE-The International Society for Optical Engineering*, vol. 6721, 2007.

[9] L. Ning, D. Chen, and C. Guan, "Two-dimension Piezoelectrical Fast Steering mirror," *Opto-Electronic Engineering*, 1995.

[10] W. Han, S. Shao, S. Zhang, Z. Tian, and M. Xu, "Design and modeling of decoupled miniature fast steering mirror with ultrahigh precision," *Mechanical Systems and Signal Processing*, vol. 167, Article ID 108521, 2022.

[11] Y. Wan, H. Xiong, T. Song et al., "Design of a fast steering mirror driven by piezoelectric ceramics," *Optical Engineering*, vol. 61, no. 02, Article ID 024102, 2022.

[12] J. Chen, Q. Hu, Z. Lin, and H. Haiyan, "Adaptive Sliding Mode Control for Fast Steering Mirror Based on RBF Neural Network Self-Learning," in *Proceedings of the 2021 33rd Chinese Control And Decision Conference (CCDC)*, pp. 1927–1932, IEEE, Kunming, China, May 2021.

[13] S. Zhang, B. Zhang, X. Li, Z. Wang, and F. Qian, "A method of enhancing fast steering mirror's ability of anti-disturbance based on adaptive robust control," *Mathematical Problems in Engineering*, vol. 2019, no. 1, pp. 1–9, Article ID 2152858, 2019.

[14] H. Wang, Q. Bao, W. Yang, and L. Zidong, "Sensor Fault Tolerant Control of a Fast Steering Mirror System Using Adaptive PI-Based Sliding Mode Observer and Hardware redundancy," *Mathematical Problems in Engineering*, vol. 2015, Article ID 918456, 2015.

[15] Z. Li, C. Song, J. Huang, and L. Xiaofei, "Influence analysis of electromechanical servo system parameters on photoelectric stability circuit," in *Proceedings of the 2021 International Conference on Computer Engineering and Artificial Intelligence (ICCEAI)*, pp. 507–510, IEEE, Shanghai, China, August 2021.

[16] C. Song, Z. Q. Li, and Z. Li, "Influence of friction on servo control performance of photoelectric stabilized platform based on time domain characteristic analysis," in *Proceedings of the 2nd International Conference on Mechanical, Electronics, and Electrical and Automation Control (METMS 2022)*, pp. 528–533, Guilin, China, April 2022.

[17] R. Matušů, B. Senol, B. B. Alagoz, and P. Libor, "Design of Robust PI Controllers for Interval Plants with Worst-Case

Gain and Phase Margin Specifications in Presence of Multiple Crossover Frequencies," *IEEE Access*, vol. 10, 2022.

[18] Y. R. Pan, Y. T. Shih, R. H. Horng, and A. C. Lee, "Advanced parameter identification for a linear-motor-driven motion system using disturbance observer," *International Journal of Precision Engineering and Manufacturing*, vol. 10, no. 4, pp. 35–47, 2009.

[19] S. Komada, N. Machii, and T. Hori, "Control of redundant manipulators considering order of disturbance observer," *IEEE Transactions on Industrial Electronics*, vol. 47, 2000.

[20] S. Sakaino, T. Sato, and K. Ohnishi, "Force-based disturbance observer for dynamic force control and a position/force hybrid controller," *IEEJ Transactions on Electrical and Electronic Engineering*, vol. 8, no. 5, pp. 505–514, 2013.

[21] Z. Gao, "Active Disturbance Rejection Control: A Paradigm Shift in Feedback Control System design," in *Proceedings of the American Control Conference*, Minneapolis, MN, USA, June 2006.

[22] M. Lian, Z. Y. Han, and F. U. Hong-Ya, *Application of Active Disturbances Rejection Control Technique to Satellite Attitude Simulation system*, Optics and Precision Engineering, Harbin, China, 2010.

[23] W. Pan, H. Xiao, and C. Wang, "Design of Ship Course Controller Based on Optimal Active Disturbance Rejection Technique," in *Proceedings of the International Conference on Intelligent System Design & Engineering Application*, Changsha, China, October 2010.

[24] J. Q. Han, "From PID Technique to Active Disturbances Rejection Control Technique," *Basic Automation*, vol. 56, no. 3, pp. 900–906, 2002.

[25] Y. Deng, J. Wang, H. Li, L Jing, and T Dapeng, "Adaptive sliding mode current control with sliding mode disturbance observer for PMSM drives," *ISA Transactions*, vol. 82, pp. 113–126, 2018.

[26] Z. Junbo, "Dynamic State Estimation with Model Uncertainties Using H-Infinity Extended Kalman Filter," *IEEE Transactions on Power Systems*, vol. 33, no. 1, pp. 1099-1100, 2018.

[27] H. Sun, R. Madonski, S. Li, and Y Zhang, "Composite control design for systems with uncertainties and noise using combined extended state observer and Kalman filter," *IEEE Transactions on Industrial Electronics*, vol. 69, no. 04, pp. 4199–4128, 2021.

[28] X. Li, Lu Wang, X. Xia, Y. Liu, and B. Zhang, "Iterative learning-based negative effect compensation control of disturbance to improve the disturbance isolation of system," *Sensors*, vol. 22, no. 9, p. 3464, 2022.

[29] B. Yao, F. Bu, J. Reedy, and G. T. C Chiu, "Adaptive robust motion control of single-rod hydraulic actuators: theory and experiments," *IEEE*, vol. 5, no. 1, pp. 79–91, 2002.

[30] B. Yao and M. Al-Majed, "High-performance robust motion control of machine tools: an adaptive robust control approach and comparative experiments," *IEEE*, vol. 2, no. 2, pp. 63–76, 1997.